Danijela Živojinović[1], Aleksandar Sedmak[2], Aleksandar Grbović[2]

CRACK GROWTH ANALYSIS IN FRICTION STIR WELDED JOINT ZONES USING EXTENDED FINITE ELEMENT METHOD

ANALIZA RASTA PRSLINE U ZONAMA SPOJA FRIKCIONO ZAVARENOG MEŠANJEM KORIŠĆENJEM PROŠIRENE METODE KONAČNIH ELEMENATA

Originalni naučni rad / Original scientific paper
UDK /UDC: 621.791.05: 669.715
621.791.05:539.4
Rad primljen / Paper received: 10.12.2013.

Adresa autora / Author's address:
[1] Technical College, bul. Zorana Djindjića 152-a Belgrade, Serbia, danijela.zivojinovic@yahoo.com
[2] University of Belgrade, Faculty of Mechanical Engineering, Belgrade, Serbia

Keywords
- aluminium
- crack
- fracture
- friction stir welding (FSW)
- extended finite element method (XFEM)
- fatigue

Ključne reči
- aluminijum
- prslina
- lom
- frikciono zavarivanje mešanjem (FSW)
- proširena metoda konačnih elemenata (XFEM)
- zamor

Abstract

Presented in this paper is the analysis of crack growth in zones of a welded joint, obtained by Friction Stir Welding - FSW. Plates of aluminium alloy 2024-T351 are frontally welded using the FSW procedure. Plate models are made using ABAQUS software. Material properties in the weld zones are adopted from papers by other authors. The plate is subjected to tensile fatigue loading with cycle asymmetry factor of R = 0. The crack growth is observed (for a non-stationary crack) and stress intensity factors are analysed around the crack tip for every crack front. The eXtended Finite Element Method (XFEM) in this analysis has enabled automatic mesh generation around the crack tip for every step of its growth. The aim of this paper is the integrity assessment of a structure that is produced by friction stir welding with an initial crack.

Izvod

U ovom radu je prikazana analiza rasta prsine u zonama zavarenog spoja izvedenog postupkom frikcionog zavarivanja mešanjem (FSW). Ploče od legure aluminijuma 2024-T351 su sučeono zavarene primenom postupka FSW. Ploče su modelirane primenom softvera ABAQUS. Osobine materijala u zonama zavarenog spoja su prihvaćene iz radova drugih autora. Ploča je podvrgnuta zamornom opterećenju zatezanjem sa faktorom nesimetričnosti ciklusa R = 0. Rast prsline je praćen (za nestacionarnu prslinu) i faktori intenziteta napona su analizirani u okolini vrha prsline za svaki front prsline. Proširena metoda konačnih elemenata (XFEM) u ovoj analizi je omogućila automatsku generaciju mreže oko vrha prsline kod svakog koraka tokom njenog rasta. Cilj ovog rada je procena integriteta konstrukcije sa inicijalnom prslinom, dobijene frikcionim zavarivanjem mešanjem.

INTRODUCTION

Structural integrity assessment represents a relatively new scientific discipline that is widely applied in the engineering practice. Calculating structural life enables the evaluation of its operational readiness. The emergence of “fail safe” design concept implies the assessment of load bearing capacity of a structural component. By detecting cracks in the structure, followed by monitoring their growth, it is possible to assess the structural integrity, i.e. component life with sufficient accuracy.

Application of new technological solutions, such as friction stir welding (FSW) enables welding of different alloys. In this way, FSW finds extensive application in various branches of industry, including aviation. Thanks to the fact that during this welding procedure, there is no melting of the material within the weld zone, the welding of aluminium alloys is made possible. This significantly reduces cost, and robust differential structures are replaced with integral structures, which leads to reduction in mass of structures, whereas connections in structural components are formed by FSW joints.

Thanks to the achievements in the field of information technologies, i.e. the development of adequate applicative software enabled an elegant approach to structural analysis. Solving current problems with stress-strain state calculation in structures with and without cracks can be performed by using some of the existing programs for this purpose, such as: Abaqus/ Morfeo, Ansys, FRANC2D/3D, NASGRO, etc. Applying the laws of fracture mechanics to a discretized system with the use of numerical methods allows for solving of existing problems. Particular attention is given to the crack growth phenomenon in structures (non-stationary cracks). The following fracture mechanics parameters are obtained that represent relevant results in the calculation: stress intensity factors – K_{I}, K_{II}, K_{III} and K_{eq} in every point of the crack front, for every step of growth. In case of fatigue load, the crack growth dependence (crack length *a*) is obtained as a function of the number of cycles of the applied load – *N*. By analyzing the results obtained in the calculation, it is possible to perform structural integrity assessment.

Owing to the emergence of a new method, the eXtended Finite Element Method – XFEM, solving of the crack growth phenomenon is significantly simplified, along with obtaining of relevant fracture mechanics parameters for each step of the crack growth.

FRICTION STIR WELDING – FSW

The friction stir welding process was patented by Wayne Thomas at TWI (The Welding Institute, Cambridge, UK) in 1991, /1/. It quickly found wide application as a very efficient welding process. In this way, it is possible to connect similar as well as different metals. FSW is the process of welding materials in a solid state. Temperatures that do not exceed the melting point of metals (400-500°C) occur in the zones of the newly formed weld. This process has found particularly significant applications in welding of aluminium alloys. This process allows welding of alloys that are not usually connected in this way (because of a considerable decrease in the quality of mechanical properties in the weld zones) up until now, which enabled the manufacturing of light structures used for transportation, such as: cars, ships, trains and airplanes.

Thus, applications of this relatively new procedure have significantly reduced the development cost. On the other hand, applying FSW produces high quality welds, with varying forms and dimensions in different materials.

Figure 1 shows the types of welded joints that can be obtained by FSW:

a) butt joint,
b) edge butt,
c) T-butt joint with three plates,
d) single lap,
e) multiple lap joint,
f) T lap joint of two plates,
g) fillet corner joint.

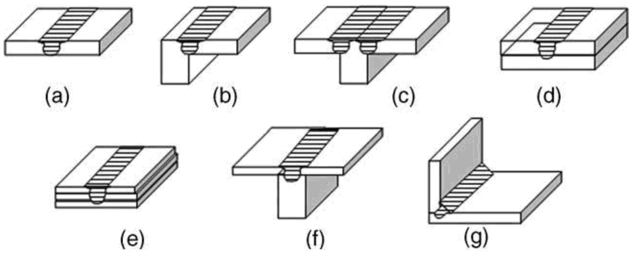

Figure 1. Types of welds obtained by FSW (image from /2/).
Slika 1. Tipovi spojeva dobijeni sa FSW (slika iz /2/)

Rotating tools that are used during the welding process penetrate the materials along the fusion line and stir the materials through their motion, thus enabling them to connect and form the weld (Fig. 2). Within the weld, the following zones exist: base material – BM; heat affected zone – HAZ; thermo-mechanically affected zone – TMAZ; and nugget - N (Fig. 3). Certain asymmetry in the welded joint cross-section in relation to the fusion line can be observed in the above figure. Two sides can be noticed: the advancing side (right) and the retreating side (left). The cause of this is the nature of material creep during the welding process. The advancing side is the one where the directions of rotation and translation velocity vectors of the tools coincide, unlike the retreating side, where these two vectors are in the opposite directions.

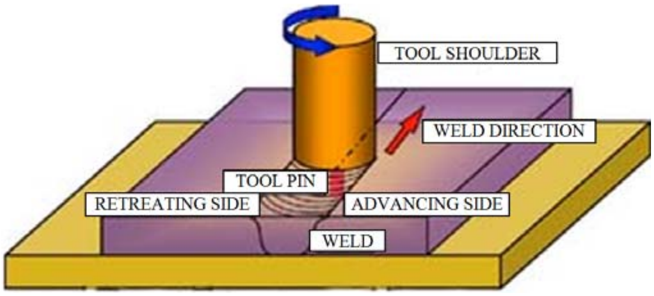

Figure 2. FSW process (image taken from /3/ and modified).
Slika 2. Postupak FSW (slika preuzeta iz /3/ i izmenjena)

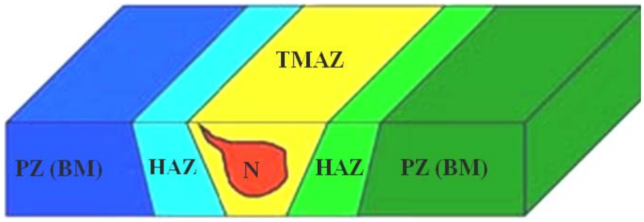

Figure 3. Cross-section of an FSW weld: a) base material (BM) or parent zone – PZ; b) heat affected zone – HAZ; c) thermo-mechanically affected zone – TMAZ; d) nugget – N – part of TMAZ, (image taken from /3/).
Slika 3. Poprečni presek FSW spoja: a) osnovni materijal (BM) ili zona – PZ; b) zona uticaja toplote – HAZ; c) zona termo-mehaničkog uticaja – TMAZ; d) grumen – N, deo TMAZ, (slika je uzeta i izmenjena iz /3/)

EXTENDED FINITE ELEMENT METHOD – XFEM

Applying the Finite Element Method (FEM) gave a significant contribution to the solving of numerous engineering problems. Calculation and analysis of stress-strain states in structures enabled high quality structural integrity assessment. This is especially significant in the structural analysis of relevant, i.e. load bearing components. Long and expensive laboratory tests have been replaced with much cheaper software packages for structural calculations. Application of numerical methods on discretized 3D and 2D models of structures that enabled solving of aforementioned problems in a very comfortable way.

The process of structural integrity assessment by using the simulation consists of the following stages:

1. development of 2D or 3D models, using available software
2. defining materials, i.e. the mechanical properties
3. determining the load spectrum (type and intensity of the load, along with its location)
4. defining boundary conditions (connections with the rest of the structural assembly)
5. generating a mesh of finite elements, where it is important to choose the appropriate element type, as well as the density of the mesh. In other words, the mesh should

be finer in areas around the initial crack and the expected propagation.

In case of the calculation of a non-stationary crack, i.e. when its growth in the structure is observed, the application of this method is not simple. The reason for this is that every step requires performing the finite element fracture in the area around the tip of the previously formed crack, and then a generation of a new finite element mesh in the same region. Hence, the application of FEM becomes noticeably more complicated. However, this method has recently been advanced by developing the so-called extended finite element method (XFEM). Automatic mesh generation with each new step in crack growth has given significant results.

XFEM is based on the correction of existing displacement equations in mesh nodes by using special Heavyside functions whose application is limited to the region around the crack tip.

XFEM SOFTWARE APPLICATIONS – ABAQUS/ MORFEO (EXAMPLES)

Fracture criteria in Abaqus

In Abaqus for XFEM simulations, two different types of elements are used /4/:

- tetrahedron, Fig. 4a and b;
- hexahedron, Fig. 4c.

In crack growth analysis, it is important to define the fracture criteria. Five different criteria exist:

1. criteria: critical stress on certain distance from the crack tip;
2. criteria: critical values of crack opening displacement;
3. criteria: dependence of crack length with time, $a = f(t)$;
4. criteria: VCCT – the Virtual Crack Closure Technique,
5. criteria: dependence of *da/dN* based on Paris law.

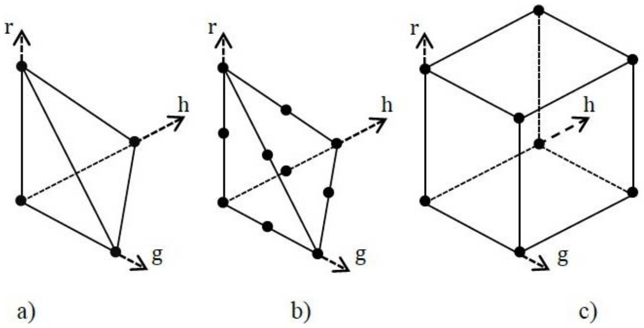

Figure 4. Finite elements for XFEM: a) linear hexahedron element-C3D6; b) second order tetrahedron element-C3D10; c) first order hexahedron element-C3D8R, (image taken from /4/).
Slika 4. Konačni elementi za XFEM: a) linearni heksaedar C3D6; b) tetraedar drugog reda C3D8R; c) heksaedar prvog reda C3D8R, (slika je uzeta iz /4/)

Material properties in FSW zones

Analysed in this paper is the crack propagation in the zones of an FSW welded joint obtained by butt welding of two thin plates. Plates are made of aluminium alloy 2024-T351.

Figure 5 shows the zones within the FSW joint. Four zones can be distinguished.

For each of these zones, the mechanical properties of the materials are defined. Values are given in Tables 1, 2 and 3.

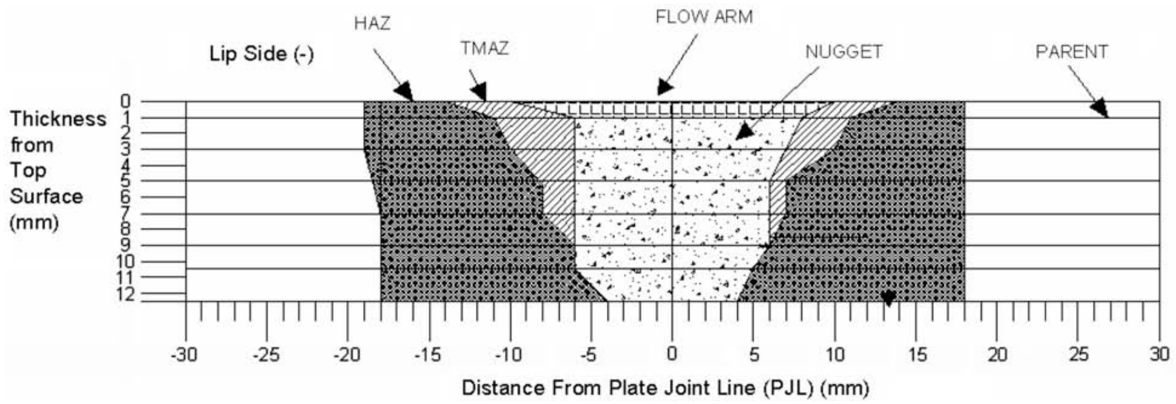

Figure 5. Cross-section of an FSW welded joint of two plates made from aluminium alloy 2024-T351, (image taken from /5/).
Slika 5. Poprečni presek FSW spoja dve ploče od legure aluminijuma 2024-T351, (slika je uzeta iz /5/)

Table 1. Material properties in FSW zones for Al alloy 2024-T351 (taken and modified from /6/).
Tabela 1. Osobine materijala u zonama FSW kod legure Al 2024-T351, (uzeto iz literature /6/)

FSW zone	nugget	TMAZ	HAZ	PZ
Young's modulus of elasticity E (MPa)	68 000	68 000	68 000	68 000
Poisson's coefficient ν (–)	0.33	0.33	0.33	0.33
yield stress σ_t (MPa)	350	272	448	370
strain hardening coefficient α (–)	–	800	719	770
strain hardening exponent n (–)	–	0.1266	0.05546	0.086
hardness HV	142	118	167	132
residual stress σ (MPa)	–41	95	–20	0

Table 2. Stress–relative strain σ–ε data in FSW zones for Al alloy 2024-T351 (taken from /6/ and modified).
Tabela 2. Napon–relativna deformacija σ–ε unutar zona FSW kod legure Al 2024-T351 (preuzeto iz /6/ i modifikovano)

nugget		TMAZ		HAZ		PZ	
σ (MPa)	ε (%)	σ (MPa)	ε (%)	σ (MPa)	ε (%)	σ (MPa)	ε (%)
30.43	0.00044	50.34	0.00070	25	0.00040	20	0.0003
51.30	0.00080	75.86	0.00123	35	0.00060	40	0.0006
69.56	0.00120	106.90	0.00160	58	0.00100	45	0.0009
91.30	0.00150	131.03	0.00200	83	0.00126	90	0.0014
130.43	0.00210	186.21	0.00310	95	0.00150	125	0.0021
186.95	0.00320	268.96	0.00450	130	0.00200	220	0.0034
286.96	0.00430	331.03	0.00570	175	0.00280	300	0.0050
331.91	0.00550			280	0.00438	320	0.0058
				330	0.00558	440	0.0084
				480	0.00898	487	0.0120
				540	0.01166		

Table 3. Constants in the Paris equation determined by: Bussu and Irwin (2003), Ali et al. (2008) and the regression calculation in FSW zones for Al 2024-T351 (taken and modified from /6/).
Tabela 3. Konstante u izrazu Parisa koje su odredili: Busi i Irvin (2003), Ali et al. (2008) i proračun regresione linije kod zona FSW za leguru Al 2024-T351 (preuzeto i modifikovano iz /6/)

FSW zones	Paris's model constants	Bussu-Irvin experiments	Ali experiments	regression calculations
nugget	C (cycles^{-1})	$2.02345\cdot10^{-10}$	$2.02345\cdot10^{-10}$	$2.8338\cdot10^{-12}$
	n	3.106	2.94	3.80
TMAZ	C (cycles^{-1})	$3.987\cdot10^{-10}$	$2.02345\cdot10^{-10}$	$5.5837\cdot10^{-12}$
	n	2.254	2.94	2.76
HAZ	C (cycles^{-1})	$8.41\cdot10^{-10}$	$2.02345\cdot10^{-10}$	$1.1778\cdot10^{-12}$
	n	2.28	2.94	2.79
PZ	C (cycles^{-1})	$2.035\cdot10^{-10}$	$2.02345\cdot10^{-10}$	$1.1778\cdot10^{-12}$
	n	2.4	2.94	2.94

MODELLING OF THE FSW JOINT, /7/

As an example of crack growth analysis in an FSW joint, a model obtained by butt welding of two plates is made. A 3D model of a plate with FSW zones is developed in ABAQUS software. Zone dimensions are determined based on metallographic images (Fig. 5).

Different shapes, dimensions and crack locations in FSW joints are analysed. However, further detailed analysis determined that certain limitations exist within the ABAQUS software. Thus, fracture mechanics parameters, as the final result of crack growth analysis in a structure, are possible to calculate only in the case when all points of the crack front in a given moment are located exclusively within a single region (zone). In case of a real 3D model (Fig. 6), regardless of the shape and dimensions of the initial crack, this problem occurs and is impossible to solve with software.

This leads to simplified 3D models of FSW joints. The approximation of the weld is performed by using flat zones (Fig. 7). Hence, plate dimensions are $1\times 20\times 60$ mm ($2W = 60$ mm, $t = 1$ mm). Figures 7 and 8 show the zones within a FSW welded joint. Based on the given dimensions, the 3D modelling is performed on butt welded plates using FSW joints.

An initial crack with a length $2a_0 = 3$ mm is introduced into the TMAZ zone. The right end of the crack is located at a distance of 1 mm from the N-TMAZ border. Further propagation of the crack through all zones in the weld is observed.

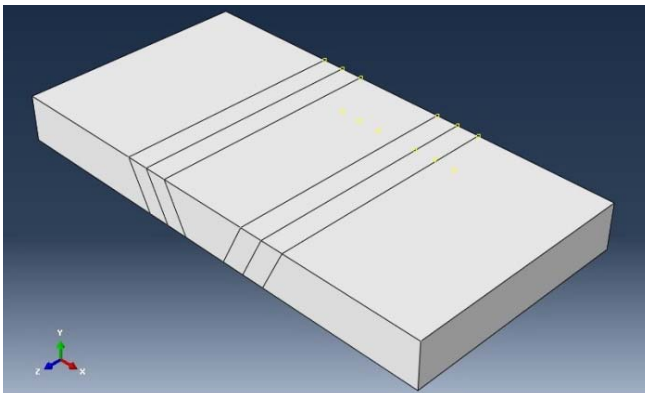

Figure 6. 3D model of a FSW welded joint (taken from /7/).
Slika 6. 3D model FSW zavarenog spoja (preuzeto iz /7/)

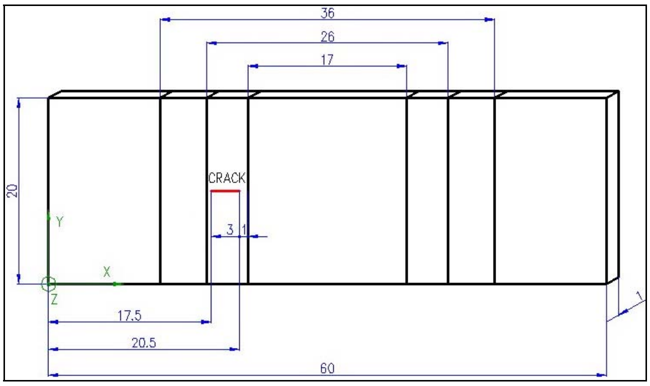

Figure 7. Simplified 3D model of FSW welded joint (from /7/).
Slika 7. Pojednostavljen 3D model FSW spoja (preuzeto iz /7/)

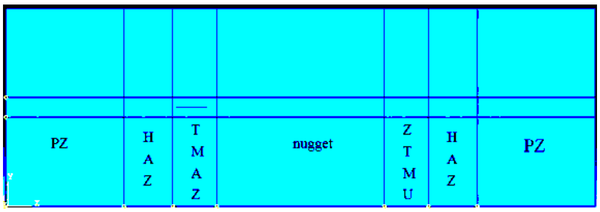

Figure 8 Zones in a FSW welded joint-3D model: NZ; TMAZ; HAZ; PZ, /7/.
Slika 8. Zone kod 3D modela FSW spoja: NZ; TMAZ; HAZ PZ, /7/

The plate is subjected to tension along the longer edge, perpendicular to the direction of the crack. The opposite parallel side is fixed (all displacements are 0), Fig. 9.

In the further calculation, the effects of fatigue tensile load are analysed, with the asymmetry load factor of $R = 0$.

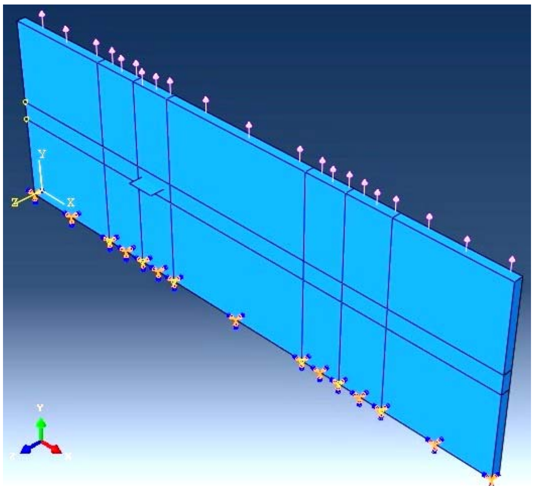

Figure 9. Defining load and boundary conditions in a simplified 3D model of a FSW welded joint, /7/.
Slika 9. Definisanje opterećenja i graničnih uslova u pojednostavljenom 3D modelu FSW spoja, /7/

For each individual zone, the characteristic properties are given: E–Young's modulus; ν–Poisson's ratio (Table 1), along with the functional dependence of stress from relative strain $\sigma = f(\varepsilon)$ (data input in ABAQUS as seen in Table 2).

All necessary parameters and material constants in the Paris equation $da/dN = C\Delta K^n$ are adopted from Table 3. Out of three offered test results, the Ali data are adopted, since further calculation (Morfeo software) requires uniquely defined values (same values for all zones within the weld).

The mesh is made of hexahedrons and is finer around the tip of the initial crack, as well as in the area of the expected growth (Fig. 10).

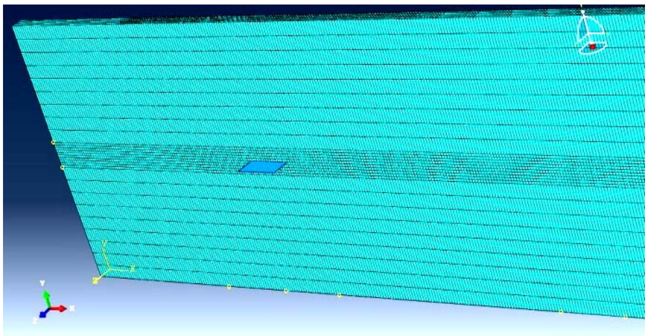

Figure 10. Finite element mesh for 3D model of FSW joint, /7/
Slika 10. Mreža 3D elemenata u modelu FSW spoja, /7/

In the following section, two cases are analysed:

1. An example of a FSW welded joint subjected to a larger tensile load.
2. An example of a FSW welded joint subjected to a smaller tensile load.

Results of calculations

FSW joint subjected to a larger tensile load

During the testing, the value of fatigue tensile load of $\sigma = -270$ MPa is used, with the load cycle asymmetry coefficient of $R = 0$. Results are presented in Tables 4-6 and Fig. 11-12.

Table 4. Numerical data: change of stress intensity factor with crack growth (right end of the crack), /7/.
Tabela 4. Numerički podaci: promena faktora intenziteta napona sa rastom prsline (desni kraj prsline), /7/

right side	x [mm]	y [mm]	K_I [MPa mm$^{0.5}$]	K_{II} [MPa mm$^{0.5}$]	K_{III} [MPa mm$^{0.5}$]	K_{ekv} [MPa mm$^{0.5}$]
step 1	20.5	10	1640.684	-77.5938	-0.21044	1643.905
step 2	20.99665	9.953149	2060.909	45.61341	1.392326	2062.726
step 3	21.49476	9.928408	2441.245	-6.82207	-1.74392	2444.124
step 4	21.99259	9.901152	2907.369	17.86187	-1.01944	2915.777
step 5	22.49102	9.879996	3324.881	33.62505	-0.00678	3327.514
step 6	22.98924	9.868938	3883.201	-1.79693	0.60412	3886.936
step 7	23.48818	9.857436	4428.728	62.43297	5.138088	4432.643
step 8	23.98639	9.86013	5237.603	-42.173	13.5333	5237.653
step 9	24.48492	9.854845	5991.541	131.3985	25.55744	5993.653
step 10	24.98179	9.870828	7278.745	-109.031	58.668	7286.111
step 11	25.48091	9.872784	8623.602	185.5499	103.903	8621.301
step 12	25.97826	9.894668	10891.17	-230.864	208.5809	10916.72
step 13	26.477	9.89828	13592.26	435.9731	438.7179	13643.53
step 14	26.97389	9.9289	21069.81	-707.284	1358.141	21263.36
step 15	27.47123	9.936958	42248.33	2087.89	4109.191	43097.35
step 16	27.94816	9.974976	284808.688	-14694.2	52252.51	299766.19
step 17	28.43	9.95	865869.38	108709.83	248106.56	986412.63

Table 5. Numerical data: change of stress intensity factor with crack growth (left end of the crack), /7/.
Tabela 5. Numerički podaci: promena faktora intenziteta napona sa rastom prsline (levi kraj prsline), /7/

left side	x [mm]	y [mm]	K_I [MPa mm$^{0.5}$]	K_{II} [MPa mm$^{0.5}$]	K_{III} [MPa mm$^{0.5}$]	K_{ekv} [MPa mm$^{0.5}$]
step 1	17.5	10	1615.404	124.228	-0.00243	1626
step 2	17.02134	10.07319	1793.62	-85.8263	-0.09357	1796.471
step 3	16.68774	10.09192	2019.982	27.68168	-0.50761	2021.031
step 4	16.40285	10.1158	2282.087	25.74527	-0.52867	2284.184
step 5	16.15932	10.14185	2621.82	-12.1396	-0.96479	2623.764
step 6	15.91271	10.16586	2952.643	32.11474	4.789943	2954.582
step 7	15.69115	10.19226	3329.472	-6.90492	-1.25086	3330.886
step 8	15.4773	10.2169	3629.493	147.8292	0.116018	3638.174
step 9	15.30967	10.25004	4115.839	24.65755	-2.63174	4126.79
step 10	15.1486	10.28326	4836.55	3.284201	-0.61036	4839.755
step 11	15.00173	10.31253	5513.954	117.5296	-3.59793	5525.685
step 12	14.87289	10.34433	6719.394	142.5377	-4.33185	6703.71
step 13	14.75668	10.37828	8483.46	99.99097	-17.7152	8447.651
step 14	14.63855	10.41613	12076.9	1044.464	-43.416	12170.17
step 15	14.55109	10.4613	28318.69	139.9859	-91.6222	28282.64
step 16	14.42	10.53	197546.6	-5527.51	-592.29	199939.4
step 17	14.28639	10.58844	784391.2	-24283.81	-3679.525	788557.4

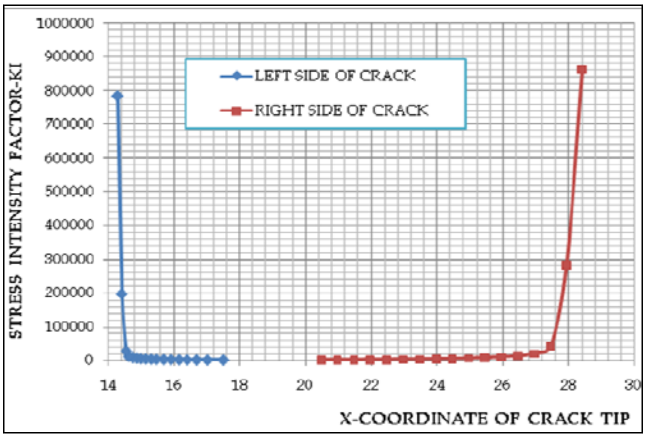

Figure 11. Change of stress intensity factor with crack growth, /7/.
Slika 11. Promena faktora intenziteta napona sa rastom prsline, /7/

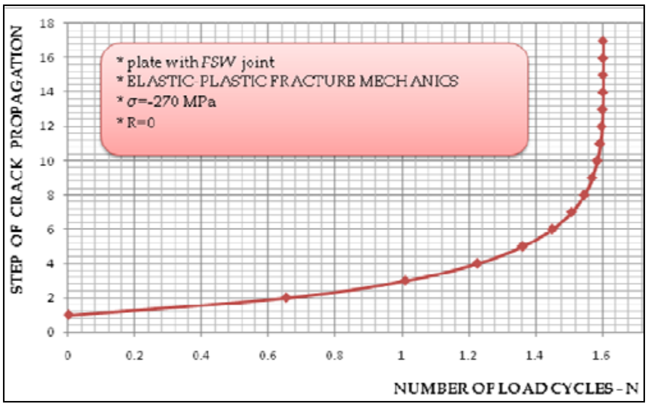

Figure 12. Crack propagataion vs. load cycle number, *N*, /7/.
Slika 12. Rast prsline prema broju ciklusa opterećenja, *N*, /7/

By analyzing the obtained data, it can be concluded that the left end of the crack propagated into the next zone (heat affected zone–HAZ), whereas the right end propagated into the N zone (Nugget). Significant increase in stress intensity factor occurs very quickly (diagrams in Fig. 11-12), which induces quick crack growth.

A sudden increase in crack length at a very low number of load cycles can be noticed, as a result of applying a high value of tensile load, $\sigma = -270$ MPa.

Table 6. Crack propagation vs. load cycle number, *N*, /7/.
Tabela 6. Rast prsline prema broju ciklusa opterećenja, *N*, /7/

step	deltaN	N
1	0.0000	0.0000
2	0.6530	0.6530
3	0.3573	1.0102
4	0.2161	1.2264
5	0.1354	1.3618
6	0.0890	1.4508
7	0.0580	1.5088
8	0.0378	1.5466
9	0.0239	1.5705
10	0.0150	1.5856
11	0.0087	1.5943
12	0.0050	1.5993
13	0.0025	1.6018
14	0.0011	1.6029
15	0.0003	1.6032
16	0.0000	1.6032
17	0.0000	1.6032

FSW joint subjected to lower values of tensile load

In the further analysis, the effect of high-cycle load is observed, for a tensile load value of $\sigma = -10$ MPa. By applying lower values of tensile load, the structure can be subjected to a larger number of load cycles, *N*, before an unstable crack growth occurs, that would lead to fracture. Results in Figs. 13a–f show a comparative overview between:
1. An undeformed model with an initial crack,
2. An undeformed model with a crack at a given moment (step), and
3. A deformed model with a crack in a given moment (step) with Mises stress distribution.

Results for FSW joint subjected to lower values of tensile load are also given in Tables 7-9 and Fig. 14-15.

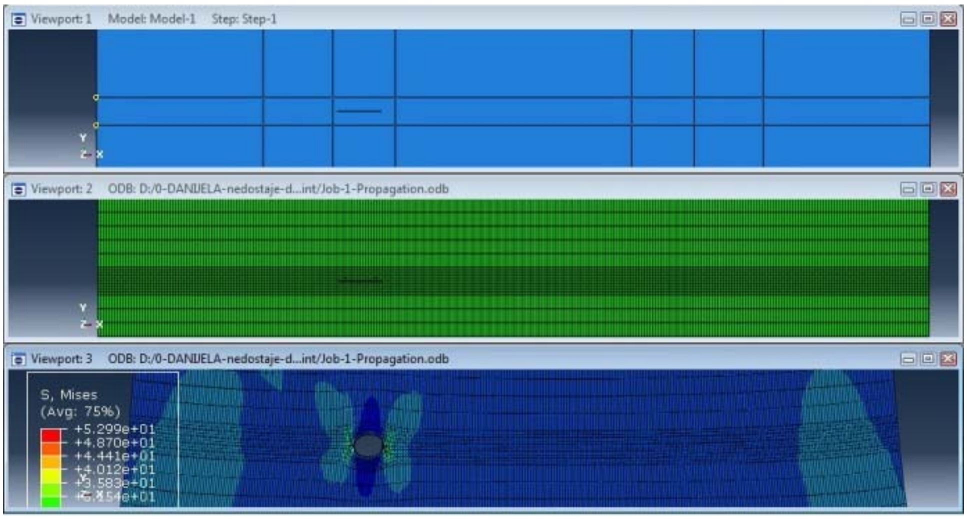

Figure 13a. Finite element mesh of 3D model of FSW joint with initial crack of length $2a_0 = 3$ mm.
Slika 13a. Mreža konačnih elemenata 3D modela FSW spoja sa inicijalnom prslinom dužine $2a_0 = 3$ mm

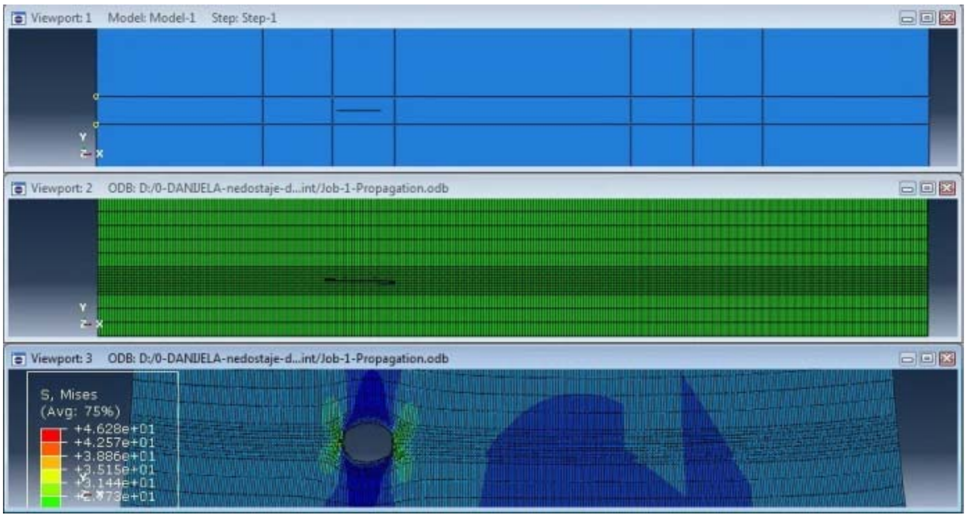

Figure 13b. Finite element mesh of 3D model of FSW. Step 2–during crack progression $\Delta a_{max} = 2$ mm.
Slika 13b. Mreža konačnih elemenata 3D modela FSW. Korak 2– tokom napredovanja prsline $\Delta a_{max} = 2$ mm

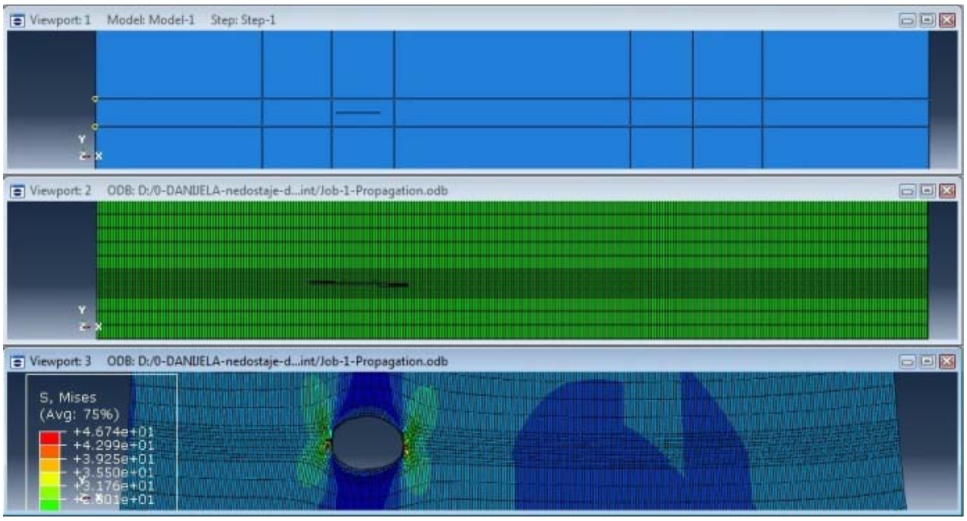

Figure 13c. Finite element mesh of 3D model of FSW. Step 4–during crack progression $\Delta a_{max} = 4$ mm.
Slika 13c. Mreža konačnih elemenata 3D modela FSW. Korak 4– tokom napredovanja prsline $\Delta a_{max} = 4$ mm

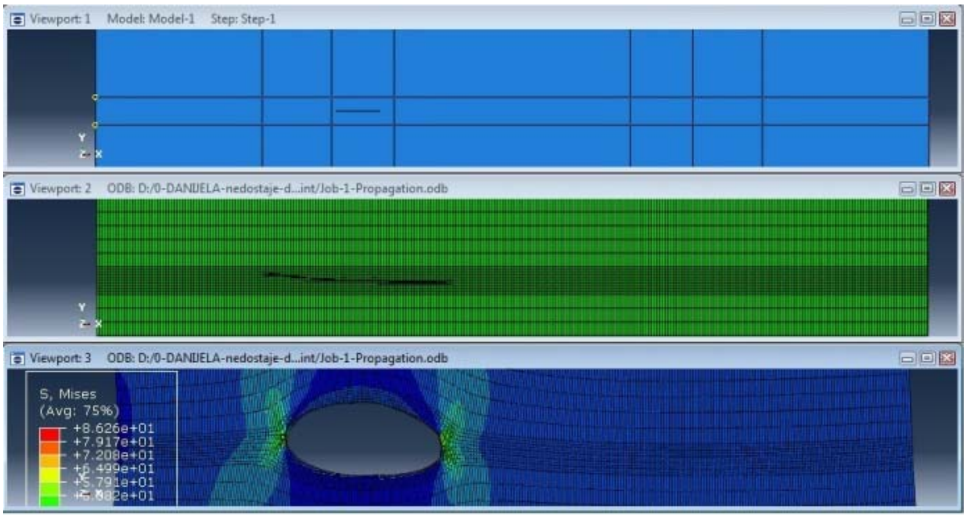

Figure 13d. Finite element mesh of 3D model of FSW. Step 11–during crack progression Δa_{max} = 11 mm.
Slika 13d. Mreža konačnih elemenata 3D modela FSW. Korak 11– tokom napredovanja prsline Δa_{max} = 11 mm

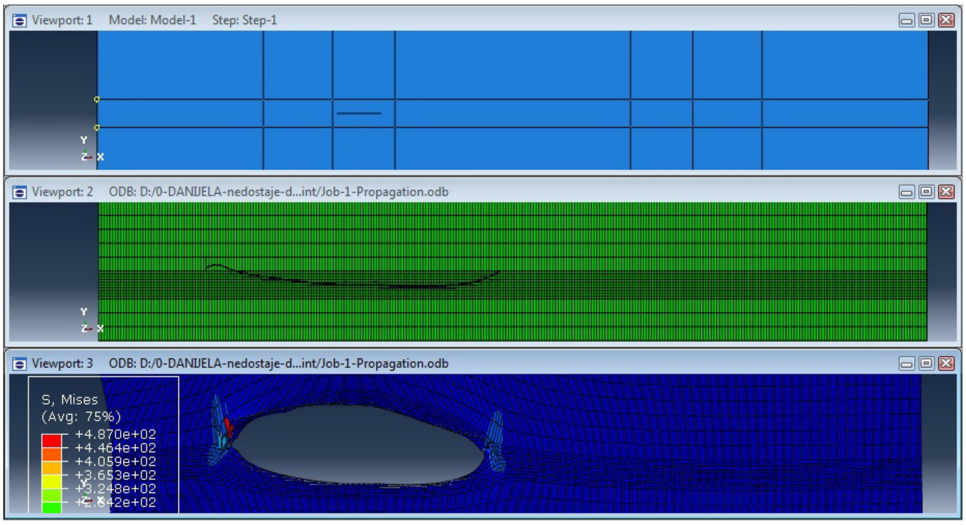

Figure 13e. Finite element mesh of 3D model of FSW. Step 20–during crack progression Δa_{max} = 20 mm.
Slika 13e. Mreža konačnih elemenata 3D modela FSW. Korak 20– tokom napredovanja prsline Δa_{max} = 20 mm

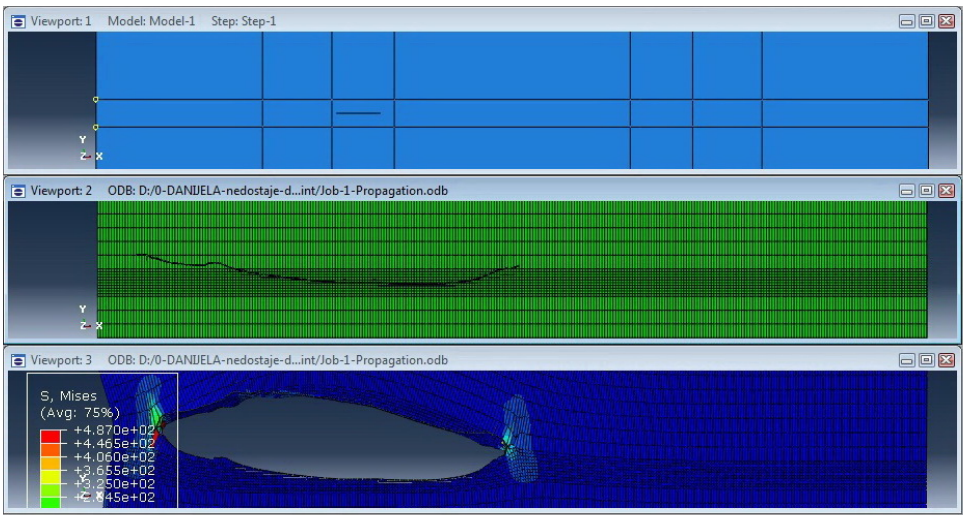

Figure 13f. Finite element mesh of 3D model of FSW. Step 31–during crack progression Δa_{max} = 31 mm.
Slika 13f. Mreža konačnih elemenata 3D modela FSW. Korak 31– tokom napredovanja prsline Δa_{max} = 31 mm

Table 7. Stress intensity factor vs. crack growth (right end), /7/.
Tabela 7. Faktora intenziteta napona – rast prsline (desni kraj), /7/

right side	x [mm]	y [mm]	K_I [MPa mm$^{0.5}$]	K_{II} [MPa mm$^{0.5}$]	K_{III} [MPa mm$^{0.5}$]	K_{ekv} [MPa mm$^{0.5}$]
step 1	20.5	10	43.48581	-1.96052	-0.00552	43.55863
step 2	20.98612	9.956274	52.06162	1.427381	0.033732	52.08641
step 3	21.43211	9.940789	59.58902	-0.1239	0.052764	59.62115
step 4	21.89227	9.922924	65.96201	0.434849	0.08367	66.02491
step 5	22.34887	9.911126	75.51936	0.183458	0.094795	72.62514
step 6	22.82828	9.901238	79.77305	0.450207	0.004949	79.84521
step 7	23.32663	9.896563	84.94474	-0.23038	0.033747	84.90827
step 8	23.78822	9.88972	91.26205	1.424903	-0.05277	91.32698
step 9	24.24095	9.897259	98.5173	0.866877	-0.0136	98.61413
step 10	24.73867	9.913889	104.1183	1.740658	0.446858	104.2098
step 11	25.20719	9.945705	110.193	0.466947	0.882754	110.3015
step 12	25.64922	9.979548	117.2795	0.613528	1.212672	117.3714
step 13	26.10868	10.01685	124.1756	2.200629	2.763993	124.3537
step 14	26.55756	10.07071	133.8298	-0.27531	3.901296	134.2827
step 15	27.01246	10.1244	141.5914	2.99464	6.271485	142.7617
step 16	27.43709	10.19144	145.6566	0.672111	11.647	148.7457
step 17	27.83959	10.24837	144.9506	1.887174	22.02354	151.1297
step 18	28.19614	10.32571	137.9345	-1.07293	35.36951	153.2248
step 19	28.51285	10.37043	122.9547	6.204732	43.28425	150.3637
step 20	28.84106	10.41073	115.2034	4.570507	47.23838	150.9562
step 21	29.10621	10.5253	107.3289	-2.13504	51.72414	149.0067
step 22	29.25215	10.60431	119.8598	-1.31871	5077484	157.766
step 23	29.41551	10.6038	121.3377	-10.5105	47.07579	168.1388
step 24	29.51848	10.58825	131.2915	15.47631	53.96088	167.559
step 25	29.61166	10.68871	109.3089	-4.11712	46.32562	165.7412
step 26	29.69397	10.70097	122.492	3.219454	60.18757	174.687
step 27	29.75515	10.73983	137.231	-5.56897	65.51063	195.8379
step 28	29.8461	10.74831	156.4098	-13.2456	64.64767	207.834
step 29	29.96207	10.77865	173.437	7.44743	74.08811	217.4187
step 30	30.11808	10.81532	177.6598	13.03324	73.34515	223.3122
step 31	30.28042	10.8298	161.6665	-4.45135	66.67891	223.8328
step 32	30.37234	10.88321	130.6031	-35.4572	40.52184	226.0398

Table 8. Stress intensity factor vs. crack growth (left end), /7/.
Tabela 8. Faktora intenziteta napona – rast prsline (levi kraj), /7/

left side	x [mm]	y [mm]	K_I [MPa mm$^{0.5}$]	K_{II} [MPa mm$^{0.5}$]	K_{III} [MPa mm$^{0.5}$]	K_{ekv} [MPa mm$^{0.5}$]
step 1	17.5	10	43.71256	2.58725	-0.0001	43.89936
step 2	17.00464	10.05845	54.02317	-1.95783	-0.01586	54.01345
step 3	16.50645	10.0808	61.18174	1.091645	-0.00089	61.35659
step 4	16.00985	10.12069	67.93631	0.4358	-0.03088	67.96648
step 5	15.51364	10.167	73.45807	0.019761	0.122614	73.46116
step 6	15.0168	10.21147	75.92496	2.844718	0.07193	78.70934
step 7	14.58384	10.26524	87.10749	-1.26861	0.040116	89.49396
step 8	14.087	10.31477	94.31271	0.721637	0.178088	95.97789
step 9	13.59221	10.37172	96.10383	0.186787	-0.00773	100.9624
step 10	13.13348	10.42626	106.1263	-1.74511	-3.22186	107.0356
step 11	12.63804	10.46308	113.1813	0.265276	-6.52358	114.9459
step 12	12.15333	10.53038	118.3953	2.776944	-10.6466	120.8648
step 13	11.67499	10.59917	125.6988	2.864039	-10.2392	128.2862
step 14	11.20161	10.67279	136.3432	0.555757	-9.9372	138.3855
step 15	10.7205	10.76169	145.9046	2.517951	-10.615	149.5756
step 16	10.25068	10.84691	153.5439	1.975566	-10.9503	156.1111
step 17	9.790916	10.94285	158.8883	4.539608	-13.8764	164.6776
step 18	9.320946	11.01656	157.4176	-1.39292	-30.4153	173.6211
step 19	8.859283	11.0018	129.0726	-6.05317	-64.9384	171.4339
step 20	8.398064	11.00328	116.5437	7.69949	-76.1535	165.0801
step 21	7.908947	11.00855	154.3143	8.477892	-68.3355	198.7575
step 22	7.483941	11.10994	190.7459	-9.90229	-45.3974	220.6202
step 23	7.001381	11.17255	199.1164	-10.3772	-55.0746	233.0691
step 24	6.632134	11.14661	190.6766	14.83453	-63.2391	230.1156
step 25	6.297473	11.19488	207.3039	11.84239	-65.5668	247.9256
step 26	5.815233	11.32751	257.438	-5.99453	-45.8372	284.4368
step 27	5.374053	11.39277	279.226	-10.3269	-21.776	298.7727
step 28	4.908677	11.45829	264.6468	9.802522	-45.5573	295.814
step 29	4.448101	11.56807	274.7561	17.64993	-50.8456	306.6074
step 30	3.996428	11.71773	262.7231	-38.4444	-77.6109	320.5178
step 31	3.561982	11.86779	262.5865	-10.4269	-112.781	321.2851
step 32	3.040136	11.91814	377.7862	72.04499	-38.7924	363.7968

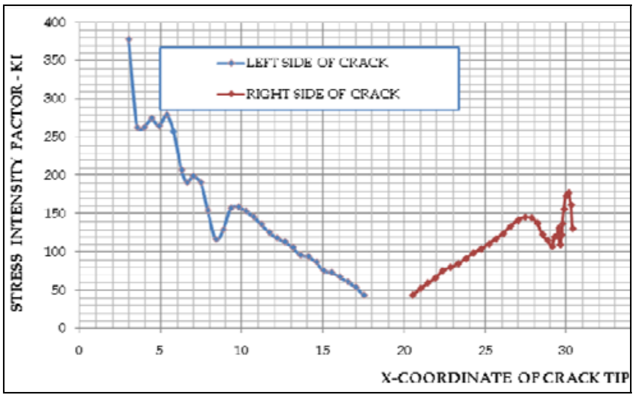

Figure 14. Change of stress intensity factor with crack growth, /7/.
Slika 14. Faktor intenziteta napona sa rastom prsline, /7/

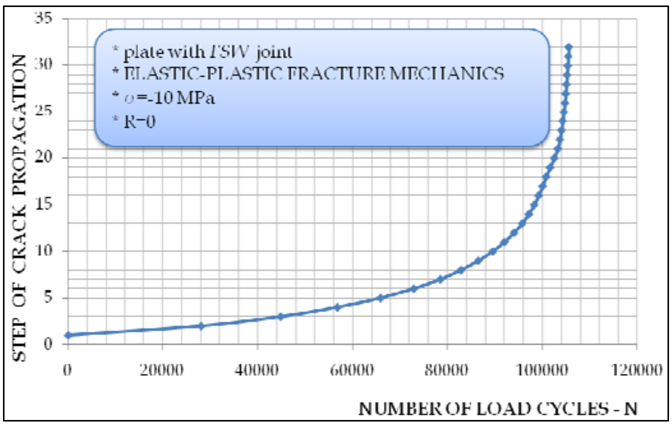

Figure 15. Crack propagation vs. load cycle number, *N*, /7/.
Slika 15. Rast prsline prema broju ciklusa opterećenja, *N*, /7/

Table 9. Crack propagation vs. load cycle number, *N*, /7/.
Tabela 9. Rast prsline prema broju ciklusa opterećenja, *N*, /7/

step	deltaN	N
1	0	0
2	28100.6	28100.6
3	16743.3	44843.9
4	11929	56772.9
5	9073.33	65846.23
6	7170.8	73017.03
7	5583.47	78600.5
8	4355.69	82956.19
9	3621.4	86577.59
10	3050.74	89628.33
11	2441.18	92069.51
12	2024.28	94093.79
13	1716.49	95810.28
14	1408.46	97218.74
15	1130.81	98349.55
16	932.906	99282.46
17	820.004	100102.5
18	742.806	100845.3
19	811.889	101657.2
20	909.797	102567
21	715.494	103282.4
22	460.387	103742.8
23	326.803	104069.6
24	248.564	104318.2
25	258.818	104577
26	220.75	104797.8
27	154.39	104952.2
28	146.934	105099.1
29	145.712	105244.8
30	135.324	105380.1
31	128.381	105508.5
32	86.1654	105594.7

CONCLUSIONS

Based on the previously presented analysis, the following conclusions are made:

- Maximum stress is formed around the crack tip and reaches its highest value in that zone (see Table 2),
- At a certain point, the crack changes its direction (deviates from the straight path), which is caused by the deforming of the structure due to fracture (crack propagation). Thus, tensile load also has a shearing component and because of that, in addition to tensile load mode I, the remaining modes (stress intensity factors, K_{II} and K_{III}) also occur.
- During the low-cycle fatigue load, after only one load cycle, significant increase in the crack growth, which is quickly followed by structural failure. Hence, the nature of the load is almost static, because of an extremely high load intensity, which leads to unstable crack growth. In case of applying lower load values, crack growth is stable until a certain number of $N \approx 80{,}000$, after which rapid crack growth leads to structural failure.

Remarks:

During the 3D modelling and application of appropriate software, it is necessary to pay attention to the following:

- Defining of boundary conditions (loads and constraints-connections with the rest of the structure or assembly).
- Designer's experience is of great importance for the mesh generating process. Thus, type and size of finite elements can significantly affect the outcome of the calculation. In addition, making the mesh finer around the crack tip, as well as the region of its expected propagation is important.

Drawbacks:

- Impossibility of obtaining relevant results for the crack front that simultaneously passes through different regions (materials with different properties) – a feature that available software (ABAQUS, FRANC) lack.
- High requirements for PC characteristics: a PC with exceptional performance: multi-core processor with a RAM capacity as high as possible.

REFERENCES

1. http://www.twi.co.uk/technologies/welding-coating-and-material-processing/friction-stir-welding/ (13.06.2013)
2. Mishra, R.S., Ma, Z.Y., *Friction stir welding and processing*, Materials Science and Engng. R 50 (2005), pp.1-78.
3. Grujičić, M., Arakere, G., Yen, C.F., Cheeseman, B.A., *Computational Investigation of Hardness Evolution During Friction-Stir Welding of AA5083 and AA2139 Aluminum Alloys*, J Materials Engng. and Perf., 2011, Vol.20, 7, pp.1097-1108.
4. Abaqus, Tutorials
5. Golestaneh, A.F., Ali, A., Zadeh, M., *Modelling the fatigue crack growth in friction stir welded joint of 2024-T351 Al alloy*, Materials and Design, 30 (2009), pp.2928-2937.
6. Golestaneh, A.F., Ali, A., Voon, W.S., Faizal, M., Mohammadi, M.Z., *Simulation of fatigue crack growth in friction stir welded joints in 2024-T351 Al alloy*, Suranaree J Sci. Technol., Vol.16 (1), 2009, pp.35-46.
7. Živojinović, D., *Primena mehanike loma na procenu integriteta zavarenih konstrukcija od legura aluminijuma*, PhD dissertation in Serbian, University of Belgrade, Faculty of Mechanical Engineering, Belgrade, 2013.